Journal of Intelligent Systems and Internet of Things
Vol. 16, No. 02, PP. 158-173, 2025
DOI: https://doi.org/10.54216/JISIoT.160212

Integrating Tent Chaotic Dung Beetle Optimization with Deep Ensemble Learning for Diabetic Retinopathy Recognition on Fundus Imaging

Arwa Darwish Alzughaibi[1], Ashrf Althbiti[2], Sultan Ahmed Almalki[3], Mohammed Al-Jabbar[3], Mohammed Alshahrani[3,*]

[1]Applied College, Taibah University, Medina, Saudi Arabia

[2]Department of Information Technology, College of Computers and Information Technology, Taif University, Taif, 21944, Saudi Arabia

[3]Computer Department, Applied College, Najran University, Najran 61441, Saudi Arabia

Emails: azughaibi@taibahu.edu.sa; a.althbiti@tu.edu.sa; Saalmalki@nu.edu.sa; mosalqahtani@nu.edu.sa; moaalshahrani@nu.edu.sa

Abstract

Diabetic Retinopathy (DR) is a general difficulty of diabetes mellitus, resulting in retina damage that affects vision. If left undetected, it has the potential to cause blindness. Regrettably, DR is irreversible, and only treatment can maintain vision. The early analysis and treatment of DR can considerably decrease the potential for visual impairment. Unlike computer-aided diagnosis (CAD) systems, the manual diagnostics method of DR retinal images by ophthalmologists is effort-, cost-, and time-consuming and liable to misdiagnoses. In present scenario, deep learning (DL) has become the classical approach that has remarkable performance in different fields, mainly in medical image classification and analysis. Convolutional neural networks (CNN) are more commonly deployed as a DL system in medical image analysis and they are very efficient. In this manuscript, we offer the design of Tent Chaotic Dung Beetle Optimization with Deep Ensemble Learning for Diabetic Retinopathy (TCDBO-DELDR) Recognition approach on Fundus Imaging. The foremost intention of the TCDBO-DELDR technique is to automate the DR detection process on fundus images via the ensemble DL model. To eradicate the noise, the TCDBO-DELDR technique initially exploits the median filtering (MF) methodology. In the TCDBO-DELDR model, the Inception v3 (IV3) model is employed for the purposes of feature extractor. For the hyperparameter tuning procedure, the TCDBO technique is used for IV3 model. Finally, the detection of DR is carried out utilizing an ensemble of three classifiers namely Deep Feedforward Neural Network (DeepFFNN), Convolutional FFNN (ConvFFNN), and Convolutional bi-directional long short-term memory (ConvBLSTM). For ensuring the enhanced efficiency of the TCDBO-DELDR system in the DR detection procedure, a widespread experimental study is prepared on the benchmark DR database. The results illustrate the superior efficiency of the TCDBO-DELDR technique with other recent DL approaches.

Received: December 30, 2024 Revised: February 25, 2025 Accepted: March 12, 2025

Keywords: Diabetic Retinopathy; Fundus Imaging; Deep Learning; Dung Beetle Optimization; Computer-Aided Diagnosis

1. Introduction

The human body experiences abnormal blood sugar levels, leading to glucose accumulation in blood vessels as it undergoes conversion into energy [1]. Diabetic retinopathy (DR) grows the patients are affected by diabetes for above 10 years. DR arises because of high blood pressure and leads to harm in the retina, and it loses the retinal vascularization that is caused by death and blindness [2]. Ophthalmologists only identify retinal vascular inflammation by performing the fundoscopy analysis, but these are costly and time-consuming. In 2030, it will be

predicted around 552 million diabetic people all over the world, and DR will become a major reason for blindness [3]. Identification and treatment of visual loss earlier is significant for avoiding visual loss. In the most serious conditions, they block blood vessels, leak fluid, or vessels swell which mains to abnormal blood vessel development and total vision loss [4]. Exudates, microaneurysms, and hemorrhages have been the major indications of DR in the retina. The shape, size, and overall construction of the lesion will determine the severity. Fundus images are an ophthalmologic screening technique for DR [5]. Avoiding diabetic-based vision loss is medically efficient and inexpensive with an automatic analysis method.

Ophthalmologists analyze the existence and harshness of the DR via a visual analysis with the help of direct inspection and assessment of the eyes [6]. For the massive count of diabetic patients worldwide, this technique is time-consuming and costly. DR harshness and earlier analysis of the disease a challenging statistics amongst experienced ophthalmologists differing extensively. Furthermore, 75 percent of patients with DR survive in underdeveloped areas but necessary ophthalmologists and the environment for identification are inaccessible [7]. World screening events are made to oppose the development of avoidable eye diseases; however, DR occurs in larger numbers for identification and treatments to DR proficiently on an individual basis. It has a requirement to automatically recognize DR by analyzing the retinal fundus images [8]. This can be described as deep learning (DL) methods to be a real-time technique for DR detection that will provide the superior identification of DR when compared to ophthalmologists. DL has a subdivision of machine learning (ML) methods, which comprises categorized layers of non-linear processing phases for unsupervised feature learning and classification patterns [9]. DL is a computer-aided diagnosis (CAD) technique. The application of the DL method in medical image analysis comprises the classification, recording of the images, segmentation, identification, and retrieval. Currently, DL is extensively employed in DR detection and classification. It will effectively learn the input data features while several combined heterogeneous sources. Numerous DL-based techniques like sparse coding constrained Boltzmann Machines, autoencoder (AE), and convolutional neural networks (CNNs). The effectiveness of such techniques improves once the number of training data rises because of the enhancement in the learned features of distinct ML techniques [10]. Besides, DL approaches are not needed the handcrafted feature extraction.

This manuscript offers the design of Tent Chaotic Dung Beetle Optimization with Deep Ensemble Learning for DR (TCDBO-DELDR) recognition approach on fundus imaging. To eradicate the noise, the TCDBO-DELDR technique initially exploits the median filtering (MF) methodology. In the TCDBO-DELDR model, the Inception v3 (IV3) technique is employed for feature extractor purposes. For the hyperparameter tuning procedure, the TCDBO technique is used for IV3 model. Finally, the detection of DR is carried out utilizing an ensemble of three classifiers namely Deep Feedforward Neural Network (DeepFFNN), Convolutional FFNN (ConvFFNN), and Convolutional bi-directional LSTM (ConvBLSTM). For ensuring the enhanced efficiency of the TCDBO-DELDR system in the DR detection procedure, a widespread experimental analysis is made on the benchmark DR database.

2. Related Works

Shamrat et al. [11] aimed to develop an automatic method of DR classification into its diverse phases employing CNN techniques. This method utilizes the effectiveness of fifteen pre-trained algorithms with the developed DR network (DRNet13) architecture. This method also differentiates the major effective system for precise DR staging dependent upon fundus imageries from 5 DR categories. Pre-processing of the image is achieved by using a median filter (MF) for Gamma correction and noise reduction. The authors [12] introduced a weighted fusion DL network (WFDLN) method. Fundus-relevant features of CLAHE images must be removed by fine-tuning the InceptionV3, while the fundus image features of CECED should be removed employing fine-tuning VGG16. The outputs of the channel have been combined in a weighted technique, and for determining the ultimate recognition outcome, the softmax classification has been exploited. Palaniswamy and Vellingiri [13] developed an IoTs-DL – DR Diagnosis (IoTDL-DRD) method that employed IoT devices to collect the data. Next, the retinal fundus imageries were pre-processed to eliminate the noises. Afterward, a mayfly optimizer-based region growing (MFORG) approach was implemented. Likewise, LSTM-based methods and DenseNet-based feature extractors have been employed for proficiently diagnosing the DR. Also, the LSTM parameter optimizer technique could be performed by the Honey Bee Optimization (HBO) technique.

In [14], a DL method was developed for categorizing DR fundus images by harshness levels, by employing ResNet and GoogleNet methods dependent upon adaptive PSO (APSO), for improved feature extractor. These feature extraction in the hybrid method can be utilized with various ML algorithms. The authors [15] projected an intellectual coyote optimizer algorithm with DL based DR detection and grading (ICOA-DLDRD) system. This technique encompasses the Gabor filtering (GF) method to eliminate the noises. Additionally, the glowworm swarm optimization (GSO) model has been employed for segmentation. In addition, SqueezeNet with CAL layer could be acquired in the feature extraction. In conclusion, COA with a DELM algorithm has been implemented. The authors [16] presented a two-phase innovative method for automatic DR classification. The primary phase employs two self-determining U-Net architectures for segmentation. During the secondary phase, the symmetric

hybrid CNN-SVD method was developed to select the more discriminative features such as OD and BV extraction through InceptionV3 dependent upon transfer learning (TL), and diagnosis of DR by identifying retinal biomarkers.

In [17], an innovative technique was presented by utilizing advanced DL methods. Significant to this method is the idea of TL. It involves the deployment of pre-existing, well-developed systems, particularly Inceptionv3 and InceptionResNetv2, for extracting the features and fine-tuning the chosen layers to provide distinctive needs of this particular diagnosis process. Simultaneously, a recently developed architecture named DiaCNN is also introduced that must be modified for the classification. Jena et al. [18] projected a new DR screening method by exploiting asymmetric DL features. The asymmetric DL features have been removed with the help of U-Net for classification of the blood vessels and optic disc. Moreover, a CNN method with an SVM approach was utilized for the DR image classification. The images can be categorized into four classes.

3. The Proposed Model

In this manuscript, we deliver the strategy of TCDBO-DELDR recognition technique on fundus imaging. The foremost intention of the TCDBO-DELDR technique is to automate the DR recognition process on fundus images via the ensemble DL model. To achieve that, the TCDBO-DELDR system has diverse types of procedures involved as MF-based image pre-processing, IV3-based feature extractor, TCDBO-based parameter tuning, and ensemble learning procedure. Fig. 1 establishes the complete flow of TCDBO-DELDR model.

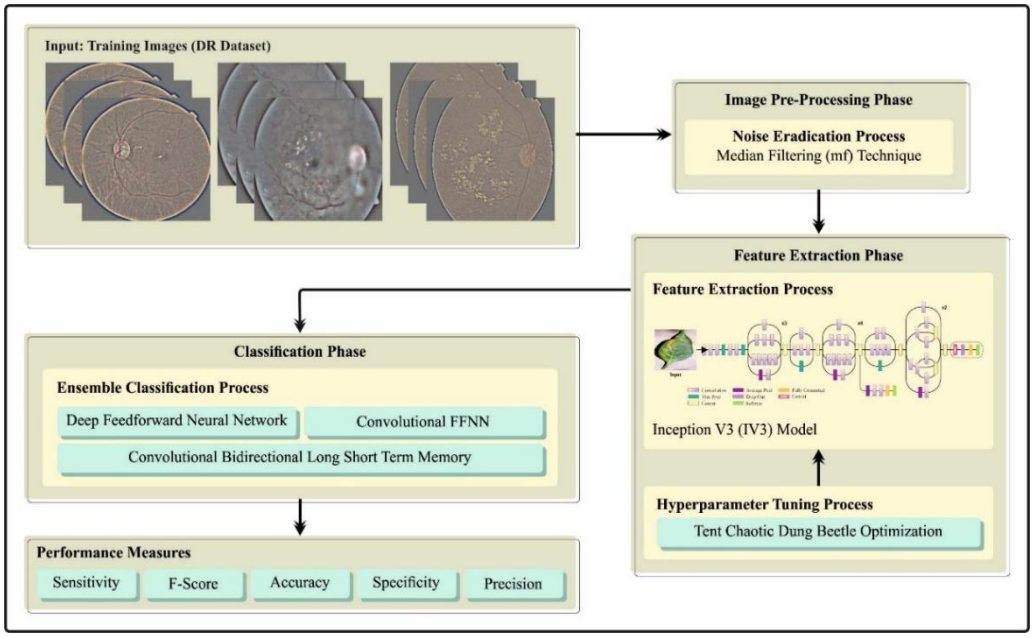

Figure 1. Overall flow of the TCDBO-DELDR methodology

A. Image Preprocessing

In an early stage, the TCDBO-DELDR system initially exploits the MF approach to eradicate the noise. MF is a classical model employed in image processing to eliminate noise while retaining edges [19]. It mechanisms by interchanging every pixel value. MF is robust to outliers since it chooses the middle value, unlike mean filtering, which calculates the average of the pixel values, making it highly efficient in scenarios with salt-and-pepper noise or impulse noise. The dimension of the neighborhood window describes the extent of filtering, with large windows providing noise reduction but blurring edges. ML finds application in several areas such as digital photography, medical imaging, and satellite imaging, where preserving image quality is essential.

B. Inceptionv3 Model

The TCDBO-DELDR technique takes place IV3 model and is utilized for feature extraction purposes. IV3 is a procedure of CNN technique particularly proposed for image and object identification [20]. It is offered as an improved procedure of the new framework of Inception, with higher effective procedure and precision of computation resources. Let accept that X is the data of input image, which contain $HxWxC$, while W denotes breadth and H refers to height, and C indicates the networks of imageries. The 1st layer of Inceptionv3 is a convolution (conv) layer with 32 filters, each dimensional 3x3x3. Considers F_1 the group of filters. The output is denoted as below:

$$Z_1 = ReLU(Conv\ (X, F_1) + b_1) \tag{1}$$

Whereas, b1 denotes the bias, $conv()$ defines the procedure of convolution, and $ReLu()$ denotes the rectified linear activation unit. A component of Inception contains multiple-branch network, which adds the outputs of many conv filters of different sizes and various available fields. The mathematical calculation is set as follows:

$$z_{(\text{inc})} = ConCat\left(\begin{bmatrix} Conv(X, F_{1\times1}), \\ Conv(X, F_{3\times3,r}), \\ Conv(X, F_{5\times5,r}), \\ \text{Max\_}Pool(X, k), \end{bmatrix}, axis = Channel\right) \tag{2}$$

Whereas decrease parameters, $F_{1\times1}$, $F_{3\times3,r}$, and $F_{5\times5,r}$ defines the filter with sizes of 1x1,3x3, and 5x5, correspondingly.

The reduction parameter is employed in order to decrease the input channel to 3x3 and 5x5 Conv that will be the rate of computational. k indicates the dimension. The outcome of Inception method is delivered over a batchnormalization (BN) layer and ReLU that set below

$$z_{(inc)} = ReLU\left(Batch\_Norm(Z_{(inc)})\right) \tag{3}$$

Then the Inception component is motivated by using a global average-pooling layer for decreasing the spatial sizes of the resultant tensor and then 2 fully connected (FC) layers with neurons of 2048:

$$z_{(fc1)} = ReLU\left(\left(W_{Fc1} * Global\_Avg\_Pool(Z_{(inc)})\right) + b_{Fc1}\right) \tag{4}$$

$$z_{(fc2)} = ReLU\left(\left(W_{Fc2} * z_{(fc1)}\right) + b_{Fc2}\right) \tag{5}$$

Now $W_{Fc1}\ and\ W_{Fc2}$ signify the weight matrices, which is connected with FC layers for the previous layer, b_{Fc1}, and b_{Fc2} define the bias, and $Global\_Avg\_Pool()$ represents the function, which norms the mapping features over the spatial length. Lastly, the equation is given below

$$Y = SoftMax\left(\left(W_{SM} * z_{(fc2)}\right) + b_{SM}\right) \tag{6}$$

Whereas W_{SM} means the weighted matrix that connects the softmax layer, and b_{SM} signifies the bias.

C. Hyperparameter Tuning using TCDBO

For the hyperparameter tuning procedure, the TCDBO model is used for IV3 model. The Tent mapping algorithm [21] optimizes the DBO algorithm. The DBO is a novel metaheuristic optimizer system involve in the foraging strategy of dung beetles (DB). Ball-roller, brood ball, small, and thief DBs, are four roles of DBs arranged from higher to lower fitness. A roller DB is an individual with high fitness, and its objective is to relocate the dung balls towards an appropriate place for reproduction. Female beetles moderately shift the dung balls of roller and lay the egg on it, which creates the brood ball. In contrast, thief DBs effort to take dung balls from others. The role corresponds to a position-adjusting strategy. After foraging, the fitness ranking of individuals defines its role in the following foraging. Individuals enhance the foraging behavior strategy and discover positions appropriate for the reproduction and existence of population through role assignment strategy depending on fitness ranking.

Bal-Roller DBs: DBs use to roll food balls toward a suitable place for reproduction. They roll food balls and navigate directly, guided by the polarized light, moon and sun. DBs climb onto the food balls and dance in order to find the moving way when they encounter an obstacle. The formula for updating the position of ball-roller DBs is given below:

$$x_i(t+1) = \begin{cases} x_i(t) + \alpha \cdot k \cdot x_i(t-1) + b \cdot \triangle x \\ x_i(t) + \tan(\theta) \cdot |x_i(t) - x_i(t-1)| \end{cases} ifR \geq 0.9 ifR < 0.9 \tag{7}$$

$$\triangle x = |x_i(t) - X^w| \tag{8}$$

Where $X(t)$ specifies the location information of i^{th}DBs at t^{th} iteration, $k \in [0,0.2]$ is a constant, formulated by the defection coefficient, $b \in (0,1)$ is a constant, α indicates the natural co-efficient allocated -1 or 1 values, X^w shows the global worst location, $\triangle x$ simulates the changes in light intensity. If $R \geq 0.9$ then the DBs adjust the location while encountering obstacles, and the deflection angle is represented as θ.

Brood Ball DBs: They use to relocate food balls towards the location fit for laying the egg. They move the food ball towards the novel position and lay the egg that makes a brood ball. Smaller DBs seek food near the brood ball after hatching. The calculation for upgrading the location is assumed below:

$$\begin{cases} Lb^* = \max(X^*(1 - RLb) \\ Ub^* = min(X^*(1 + RUb) \end{cases} \quad (9)$$

$$R = 1 - \frac{t}{T_{\max}} \quad (10)$$

$$x_i(t+1) = X^* + b_1 \cdot (x_i(t) - Lb^*) + b_2 \cdot (x_i(t) - Ub^*) \quad (11)$$

Here, X^* is the present local best location, Lb^* and Ub^* indicates the lower and upper bounds, $T_{\max}$ refers to maximal iteration counter, Lb and Ub are the low and up bounds of the optimization problems, the random variables b_1 and b_2 with the dimensional of $1\times D$, whereas D denotes the dimensional.

Small DBs: by rolling food balls, small DBs seek food. Some food balls raise the next generation and egg laying, while the remaining serve as a food source. The female beetle lays the egg on it and buries the food balls. The food ball provides a place for essential nourishment and larval growth. The formulation for upgrading the location of small DBs is set below:

$$\begin{cases} Lb^b = \max(X^b \times (1 - R), Lb) \\ Ub^b = \min(X^b \times (1 + R), Rb) \end{cases} \quad (12)$$

$$x_i(t+1) = x_i(t) + C_1 \cdot (x_i(t) - Lb^b) + C_2 \cdot (x_i(t) - Ub^b) \quad (13)$$

In the equations, X^b is the global optimum location, Lb^b and Ub^b refers to lower and upper bounds of the optimum hunting region correspondingly. C_1 and C_2 are the uniform distribution of random integers within $[0 \text{ and } 1]$.

Thief DBs: Few DB exhibits the behavior of theft food balls from one another. They contest with others to gain food balls for their individual.

$$x_i(t+1) = X^b + S \cdot g \cdot (|x_i(t) - X^*| + |x_i(t) - X^b|) \quad (14)$$

In Eq. (14), S is a constant value and g denotes the $1\times D$ normal distribution random vector.

The tent mapping technique is applied in Tent DBO (TDBO) algorithm. The random population is initialized in DBO leads to worst quality of population. The Tent chaotic model is used for adjusting the population since it generates Gaussian-distributed random number, which exhibits exploratory and good randomness features.

$$X_{t+1} = \begin{cases} \frac{X_t}{b}, & if\ 0 \le X_t \\ \frac{1 - X_t}{1 - b}, & if a \le X_t < 1 < a \end{cases} \quad (15)$$

In Eq. (15), X_t refers to the X value at t time, and a is a random selection from [0.5,1]. Then we set $X_0 = 0.5$. Eq. (16) is used to attain the initial value for the population. We apply Eq. (17) for normalization whose value exceeds the boundaries.

$$x_i(t) = X_t \cdot (Ub - Lb) + Lb \quad (16)$$

$$x_i(t) = \begin{cases} Lb, if\, x_i(t) < Lb \\ Ub, if\, x_i(t) > Ub \end{cases} \quad (17)$$

The TCDBO system grows a fitness function (FF) to attain improved classifier efficacy. It decides a optimistic number to define the good efficacy of candidate results. Throughout this work, the diminishing of the classifier error value was invented as FF and expressed in Eq. (18).

$$fitness(x_i) = ClassifierErrorRate(x_i) = \frac{Misclassified\ instance\ counts}{Total\ instance\ counts} * 100 \quad (18)$$

D. Ensemble Learning Process

Lastly, the recognition of DR is carried out using an ensemble of three classifiers namely DeepFFNN, ConvFFNN, and ConvBLSTM techniques.

i) DeepFFNN Model

The DeepFFNN technique was mainly intended to calculate the subsequent probability spreading of a class that specified a sentence of input containing words [22]. This method proceeds a solitary input that is signified by a vector of N-dimensional. Input is handled over a layer of projection that changes the words of input into a constant feature representation. This aids the system in getting word weight or embedding, as tackled to random word

indices. It is highly significant to notice that the layer of projection will not utilize any activation function of non-linear because its main part is to signify an input in a condensed constant space. Fig. 2 depicts the structure of DeepFFNN.

Afterward the layer of projection, the system permits the information to a hidden layer (HL). In a method of DeepFFNN, manifold HL can be used among the output and input layers to gradually remove high-level features from an input of raw. The formulation for FFNN with a solitary HL was defined by Eq. (19) which calculates the activations of HL.

The output layer employs softmax to deliver a probabilistic analysis of the output, and subsequent in-class prospects. After training, the sentence of input was considered. The objective function utilized is the probability of trained data stated in Eq. (20), whereas the total was grabbed over the training instances.

In the FFNN, learning arises over backpropagation (BP) that involves altering the linking weights to diminish the error of networks. To compute the error, a cross-entropy error condition has been used exposed in Eq. (21), which signifies the dissimilarity between the predicted and actual prospects for accurate class.

$$h_j^{(t)} = g\left(\sum_{m=1}^{n \cdot P} P_m^{(t)} W_{jm}^{(PH)} + b_j^{(H)}\right) \tag{19}$$

$$f(model) = \sum_{t=1}^{T} \log C_{p_i}^{(t)} \tag{20}$$

$$E\left(C_i^{(t)}\right) = C_{a_i}^{(t)} - C_{p_i}^{(t)} \tag{21}$$

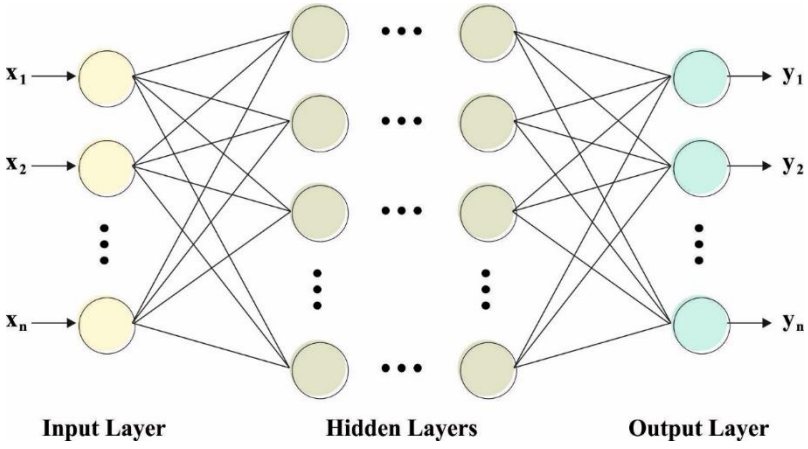

Figure 2. Architecture of DeepFFNN

ii) ConvFFNN Model

The ConvFFNN procedures its input over a sequence of filtering processes in order to make the output of the forecast. In contrast to typical FFNN, the ConvFFNN includes many layers of Conv among the output and input layers, allowing it to manage additional difficult features. Many Conv layers are included, so the system adjusts to high-level features, instead of consuming a few configurable parameters when equated to standard FFNNs. In the Conv layer, a kernel filter, signified as K, is functional to the input feature matrix X. This kernel filter moves by a definite amount of steps, executing a multiplication process of matrix on the part of X where the kernel is positioned. The Conv process has been exactly signified by Eq. (22), resulting in a 2D matrix.

The following layers naturally function on 1-D data, the 2-D output from Conv layer is compressed data which is delivered to the resultant layer. Eq. (23) displays the linear transformation, including a dot product process with weights and a bias term. Like DeepFFNN, the softmax is employed at the output layer in order to deliver a probabilistic interpretation of the system's output.

$$Z = X * K \tag{22}$$

$$Z = W^T \cdot X + b \tag{23}$$

iii) ConvBLSTM Model

Recurrent Neural Network (RNN), like LSTM networks, are best at demonstrating consecutive data. An LSTM integrates a memory cell and 3 gates such as forget, output, and input that allow it to calculate HL. These gates utilizing activation functions of sigmoid, manage the data kept from the memory cell. The present HL in a layer of LSTM was defined as dependent upon the output gate and cell state as stated in Eq. (24).

In the BLSTM layer, the last output for a word at the location is calculated as revealed in Eq. (25), connecting both the right and left recurrent HL. The right recurrent HL is calculated in a method parallel to the left one. The symbol $\oplus$ symbolizes the link of the dual HLs.

$$h_l^{(t)} = \tanh\left(c_l^{(t)}\right) \cdot o_l^{(t)} \tag{24}$$

$$z^{(t)} = \left(h_l^{(t)} \oplus h_r^{(t)}\right) \tag{25}$$

4. Result Analysis and Discussion

The performance analysis of the TCDBO-DELDR methodology takes place employing the Diabetic Retinopathy 224 x 224 Gaussian Filtered dataset [23]. It has 3662 images with 5 classes as demonstrated in Table 1. Fig. 3 illustrates the sample imageries.

Table 1: Details on database

Classes	No. of Images
"No DR"	1805
"Mild"	370
"Moderate"	999
"Severe"	193
"Proliferate DR"	295
Total Images	3662

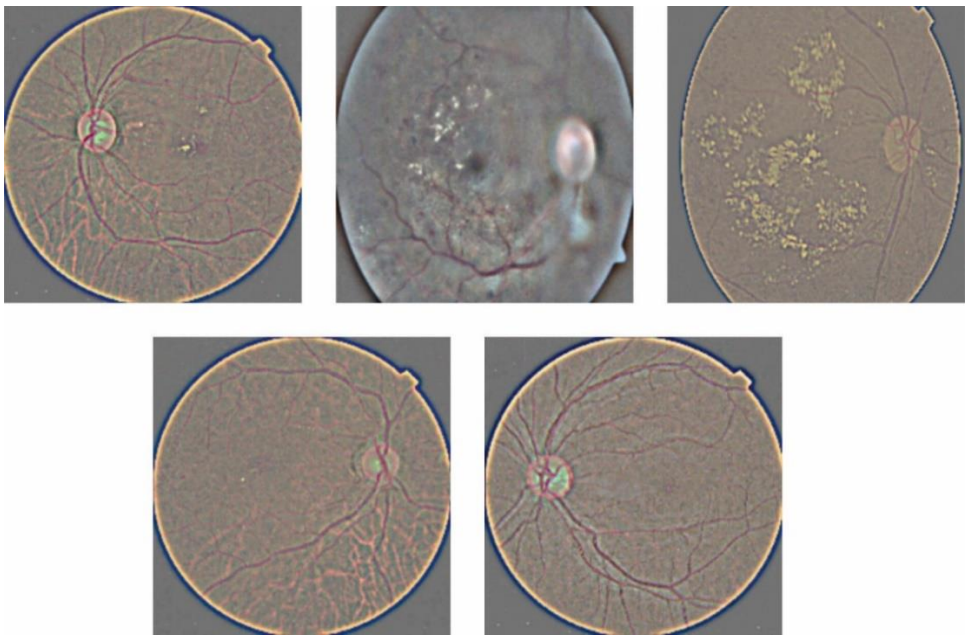

Figure 3. Sample Images

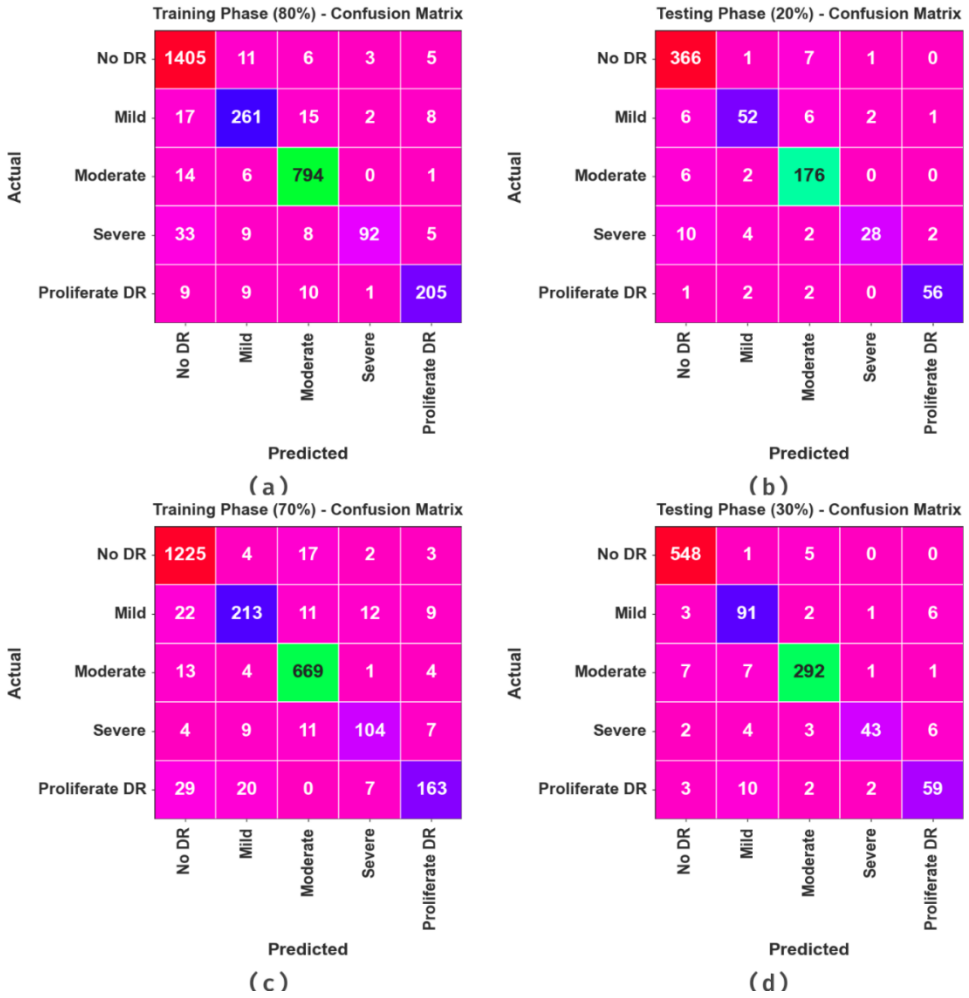

Figure 4. Confusion matrices of (a-b) 80:20 of TRAPA/TESPA (c-d) 70:30 of TRAPA/TESPA

Fig. 4 examines the confusion matrices attained by the TCDBO-DELDR system at 80:20 and 70% TRAPA and 30% TESPA. These outcomes stated that the TCDBO-DELDR has effectual recognition and classification of various stages of DR proficiently.

Table 2 and Fig. 5 represents the DR recognition performance of the TCDBO-DELDR can be studied with 80%TRAPA and 20%TESPA. The results underlined that the TCDBO-DELDR system recognizes different stages of DR proficiently. With 80%TRAPA, the TCDBO-DELDR model provides an average $accu_y$ of 97.65%, $prec_n$ of 92.79%, $sens_y$ of 86.40%, $spec_y$ of 98.21%, and F_{score} of 88.95%. Likewise, based on 20%TESPA, the TCDBO-DELDR model delivers an average $accu_y$ of 97.65%, $prec_n$ of 92.79%, $sens_y$ of 86.40%, $spec_y$ of 98.21%, and F_{score} of 88.95%.

Table 2: DR recognition outcome of TCDBO-DELDR technique with 80%TRAPA and 20%TESPA

Classes	$Accu_y$	$Prec_n$	$Sens_y$	$Spec_y$	F_{Score}
TRAPA (80%)					
No DR	96.65	95.06	98.25	95.13	96.63
Mild	97.37	88.18	86.14	98.67	87.15
Moderate	97.95	95.32	97.42	98.16	96.36
Severe	97.92	93.88	62.59	99.78	75.10
Proliferate DR	98.36	91.52	87.61	99.29	89.52
Average	97.65	92.79	86.40	98.21	88.95

TESPA (20%)					
No DR	95.63	94.09	97.60	93.58	95.81
Mild	96.73	85.25	77.61	98.65	81.25
Moderate	96.59	91.19	95.65	96.90	93.37
Severe	97.14	90.32	60.87	99.56	72.73
Proliferate DR	98.91	94.92	91.80	99.55	93.33
Average	97.00	91.15	84.71	97.65	87.30

The efficiency of the TCDBO-DELDR approach is clearly established in Fig. 6 in the method of validation accuracy (VADAC) and training accuracy (TRAAC) with 80%TRAPA and 20%TESPA. The outcome displays a useful study of the outcome of TCDBO-DELDR method over fluctuating epochs, signifying its procedure of learning and general skills. Mostly, the output concludes a steady enhancement in the VADAC and TRAAC with development in epochs. It defends the adaptive aspect of the TCDBO-DELDR system in the pattern recognition process under TES and TRA data. The amplified tendencies in VADAC outline the skill of the TCDBO-DELDR to adjust to the TRA data and exceed to provide precise identification on unnoticed data, showing strong generality skills.

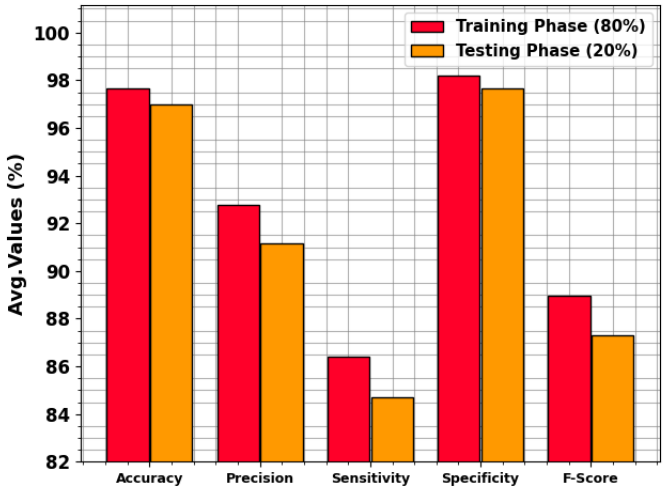

Figure 5. Average of TCDBO-DELDR approach with 80%TRAPA and 20%TESPA

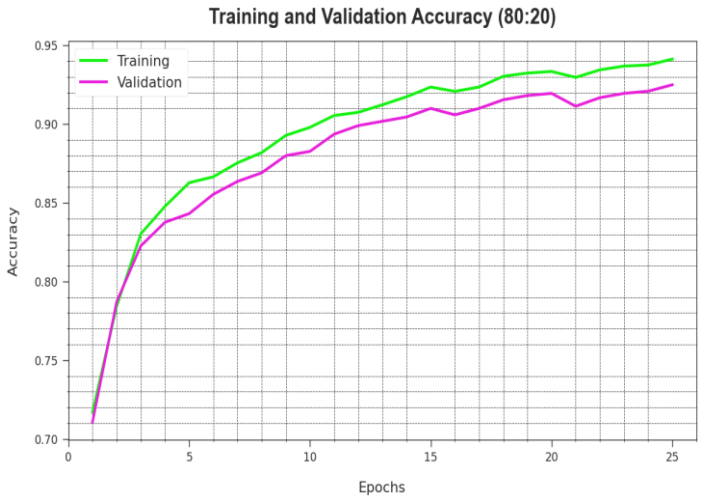

Figure 6. $Accu_y$ Curve of TCDBO-DELDR technique with 80%TRAPA and 20%TESPA

Fig. 7 depicts an entire illustration of the validation loss (VADL) and training loss (TRAL) results of the TCDBO-DELDR approach above discrete epochs with 80%TRAPA and 20%TESPA. The advanced minimizer in TRAL highpoints the TCDBO-DELDR system enlightening the weights and reducing the error of classification. The outcome identifies a clear sympathetic of the TCDBO-DELDR method related to the TRA data, underlining its ability in taking designs. Mainly, the TCDBO-DELDR model constantly increases its limitations in decreasing the alterations amongst the actual and forecast TRA classes.

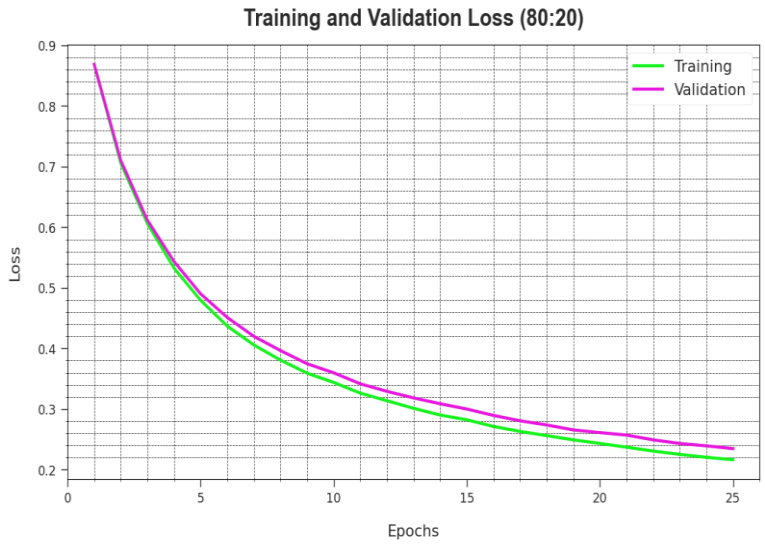

Figure 7. Loss curve of TCDBO-DELDR model at 80%TRAPA and 20%TESPA

Examining the PR graph, as exhibited in Fig. 8, the outcomes proficient that the TCDBO-DELDR method gradually achieves higher PR outcomes at each class with 80%TRAPA and 20%TESPA. It proves the heightened skills of the TCDBO-DELDR model in the classification of dissimilar class labels, exhibiting skill in the recognition classes.

Likewise, in Fig. 9, ROC graph acquired by the TCDBO-DELDR compressed in the identification of separate labels with 80%TRAPA and 20%TESPA. It gives a complete understanding of the trade-off amongst FRP and TPR over separate detection epoch counts and threshold values. The result emphasized the enhanced classifier outcomes of the TCDBO-DELDR model with each class, outlining the efficacy of overwhelming numerous identification difficulties.

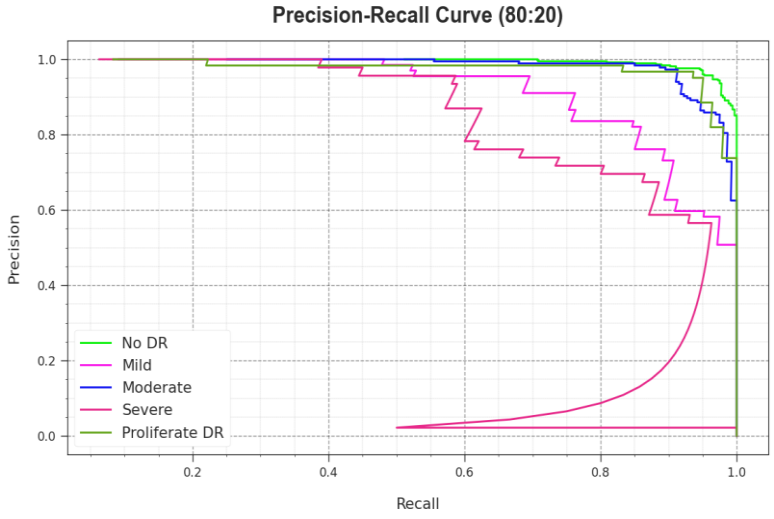

Figure 8. PR curve of TCDBO-DELDR model at 80%TRAPA and 20%TESPA

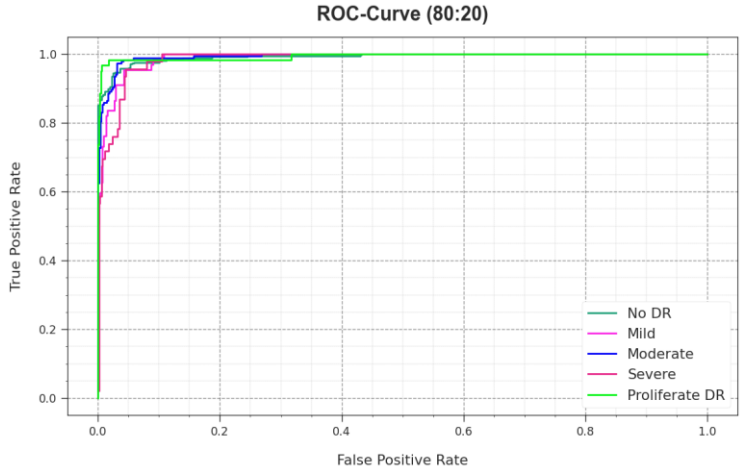

Figure 9. ROC curve of TCDBO-DELDR approach at 80%TRAPA and 20%TESPA

The DR recognition outcomes of the TCDBO-DELDR model is reported with 70%TRAPA and 30%TESPA and illustrated in Table 3 and Fig. 10. These experimental outcomes highlighted that the TCDBO-DELDR algorithm recognizes different stages of DR proficiently. Based on 70%TRAPA, the TCDBO-DELDR system offers an average $accu_y$ of 97.05%, $prec_n$ of 88.92%, $sens_y$ of 85.20%, $spec_y$ of 97.85%, and F_{score} of 86.91%. Meanwhile, in terms of 30%TESPA, the TCDBO-DELDR method gets an average $accu_y$ of 97.60%, $prec_n$ of 89.47%, $sens_y$ of 86.77%, $spec_y$ of 98.37%, and F_{score} of 87.89%, respectively.

Table 3: DR recognition outcome of TCDBO-DELDR method at 70%TRAPA and 30%TESPA

Classes	$Accu_y$	$Prec_n$	$Sens_y$	$Spec_y$	F_{Score}
TRAPA (70%)					
No DR	96.33	94.74	97.92	94.82	96.31
Mild	96.45	85.20	79.78	98.39	82.40
Moderate	97.62	94.49	96.82	97.92	95.64
Severe	97.93	82.54	77.04	99.09	79.69
Proliferate DR	96.92	87.63	74.43	99.02	80.49
Average	97.05	88.92	85.20	97.85	86.91
TESPA (30%)					
No DR	98.09	97.34	98.92	97.25	98.12
Mild	96.91	80.53	88.35	97.79	84.26
Moderate	97.45	96.05	94.81	98.48	95.42
Severe	98.27	91.49	74.14	99.62	81.90
Proliferate DR	97.27	81.94	77.63	98.73	79.73
Average	97.60	89.47	86.77	98.37	87.89

The effectiveness of the TCDBO-DELDR approach is clearly presented in Fig. 11 in the process of VADAC and TRAAC curves with 70%TRAPA and 30%TESPA. The outcome shows a appreciated clarification of the solution of TCDBO-DELDR over fluctuating epoch counts, demonstrating its learning process and general capabilities. The higher trend in VADAC summaries the aptitude of the TCDBO-DELDR model to regulate to the TRA data and also exceed to give accurate identification on unknown data, indicating out the strong general skills.

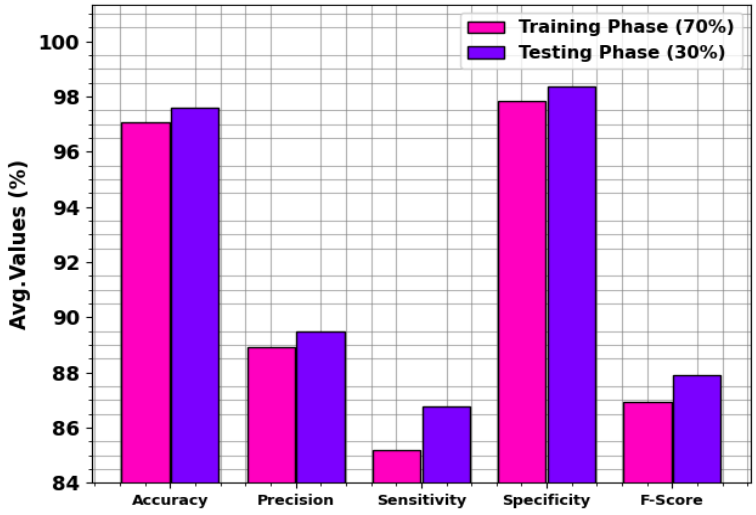

Figure 10. Average of TCDBO-DELDR at 70%TRAPA and 30%TESPA

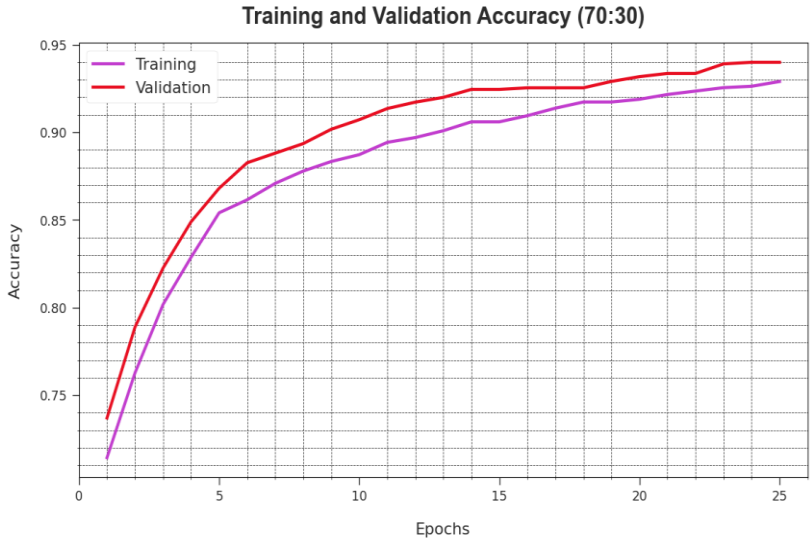

Figure 11. $Accu_y$ Curve of TCDBO-DELDR model with 70%TRAPA and 30%TESPA

Fig. 12 represents an entire illustration of the VADL and TRAL curves of the TCDBO-DELDR model over discrete epochs with 70%TRAPA and 30%TESPA. The decrease in TRAL highpoints the TCDBO-DELDR model refining the weight and lessening the classifier error. The result requires a better accepting of the TCDBO-DELDR connected with TRA data, underlining its skill in taking patterns. Significantly, the TCDBO-DELDR system frequently increases its limitations in lessening the modifications among the real and prediction outcomes.

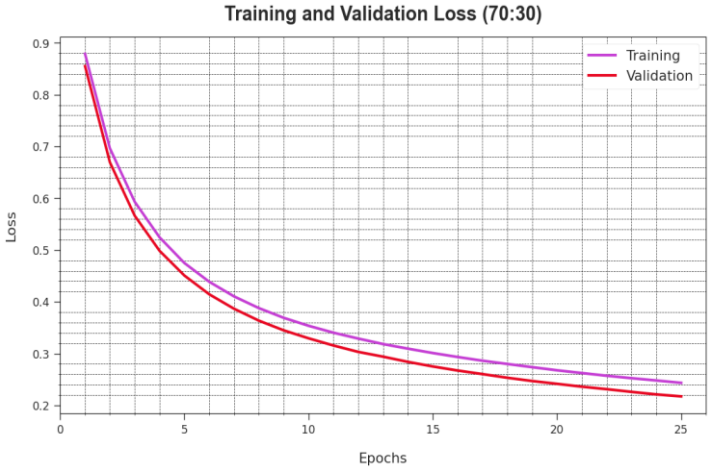

Figure 12. Loss curve of TCDBO-DELDR methodology with 70%TRAPA and 30%TESPA

Studying the PR graph, as presented in Fig. 13, the results safeguarded that TCDBO-DELDR gradually realizes enhanced PR outcomes at all classes with 70%TRAPA and 30%TESPA. It confirms the enriched proficiencies of the TCDBO-DELDR in the classification of distinct classes, representative ability in the class's detection.

Likewise, in Fig. 14, ROC graph acquired by TCDBO-DELDR outpaced the classification of various labels with 70%TRAPA and 30%TESPA. It provides a complete understanding of the trade-off between FRP as well as TPR over separate recognition threshold rate and epoch count. The result highlighted the superior classifier outcomes of TCDBO-DELDR technique with classes, outlining the efficacy for overcoming several identification difficulties.

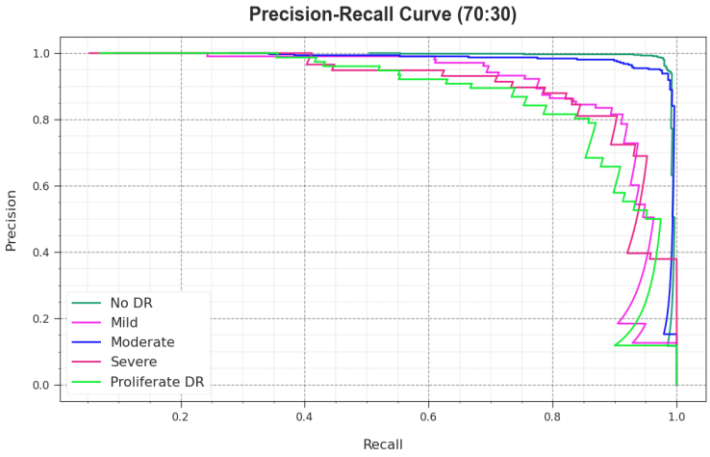

Figure 13. PR curve of TCDBO-DELDR under 70%TRAPA and 30%TESPA

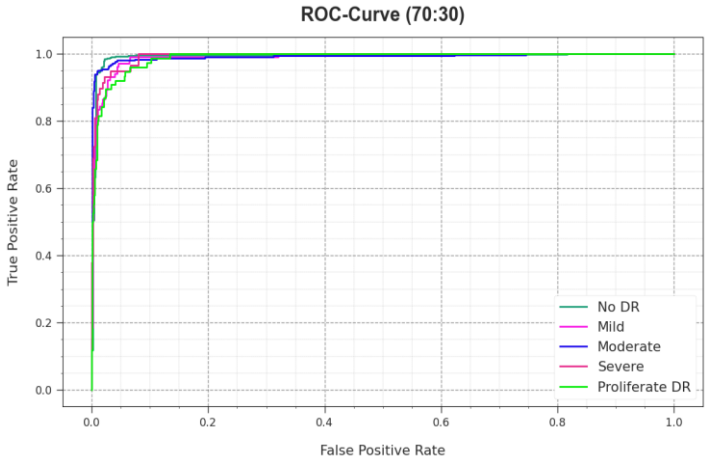

Figure 14. ROC curve of TCDBO-DELDR at 70%TRAPA and 30%TESPA

To guarantee the enhanced DR recognition outcomes of the TCDBO-DELDR method, an extensive comparison study is made in Table 4 and Fig. 15 [11]. These experimentation outcome values referred that the EfficientNet-B7 approach has revealed poorer performance with a lower $accu_y$ of 84.36%.

Table 4: $Accu_y$ outcome of the TCDBO-DELDR with other models

Methodology	Accuracy (%)
EfficientNet-B7	84.36
UNet Model	95.90
ResNet-50	95.58
CNN Algorithm	96.00
AlexNet	94.30
DRNet13	97.00
ELM Model	97.27
TCDBO-DELDR	97.65

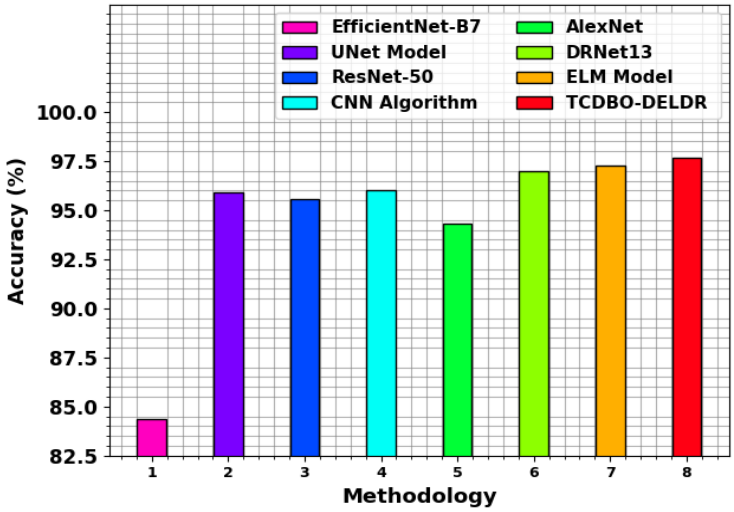

Figure 15. $Accu_y$ Analysis of TCDBO-DELDR technique with other models

In line with that, the UNet Model, ResNet-50, CNN Algorithm, AlexNet, DRNet13, and ELM Model have reported closer $accu_y$ values of 95.90%, 95.58%, 96.00%, 94.30%, 97.00%, and 97.27% respectively. Nevertheless, the TCDBO-DELDR technique accomplishes superior outcomes with $accu_y$ of 97.65%. Thus, the TCDBO-DELDR technique enables to accurately detect and classify DR stages.

5. Conclusion

In this work, we offer the project of the TCDBO-DELDR recognition model on fundus imaging. The foremost intention of the TCDBO-DELDR technique is to automate the DR recognition process on fundus images via the ensemble DL model. To achieve that, the TCDBO-DELDR technique has diverse types of procedures involved as MF-based image pre-processing, feature extractor-using IV3, parameter fine-tuning using TCDBO, and ensemble learning process. In the initial stage, the TCDBO-DELDR system initially exploits the MF approach to eliminate the noise. In the TCDBO-DELDR, the IV3 model is utilized for feature extractor purposes. For the parameter fine-tuning procedure, the TCDBO system is used for the IV3 model. Lastly, the recognition of DR is carried out using an ensemble of three classifiers namely DeepFFNN, ConvFFNN, and ConvBLSTM. For ensuring the enhanced efficiency of the TCDBO-DELDR model in the DR detection procedure, a widespread experimental outcome is prepared on the benchmark DR database. The results illustrate the superior efficiency of the TCDBO-DELDR technique with other recent DL models.

Funding: "This research received no external funding"

Conflicts of Interest: "The authors declare no conflict of interest."

References

[1] Y. Bai, X. Zhang, C. Wang, H. Gu, M. Zhao, and F. Shi, "Microaneurysms detection in retinal fundus images based on shape constraint with region-context features," *Biomed. Signal Process. Control*, vol. 85, p. 104903, 2023.

[2] R. E. Putra, H. Tjandrasa, and N. Suciati, "Severity classification of non-proliferative diabetic retinopathy using convolutional support vector machine," *Int. J. Intell. Eng. Syst.*, vol. 13, no. 4, 2020.

[3] Das, S. K. Biswas, and S. Bandyopadhyay, "A critical review on diagnosis of diabetic retinopathy using machine learning and deep learning," *Multimed. Tools Appl.*, vol. 81, no. 18, pp. 25613–25655, 2022.

[4] S. Jan, I. Ahmad, S. Karim, Z. Hussain, M. Rehman, and M. A. Shah, "Status of diabetic retinopathy and its presentation patterns in diabetics at ophthalmology clinics," *J. Postgrad. Med. Inst.*, vol. 32, no. 1, 2018.

[5] L. Andersen and P. Andersson, "Deep learning approach for diabetic retinopathy grading with transfer learning," 2020.

[6] L. Math and R. Fatima, "Adaptive machine learning classification for diabetic retinopathy," *Multimed. Tools Appl.*, vol. 80, no. 4, pp. 5173–5186, 2021.

[7] He, T. Li, N. Li, K. Wang, and H. Fu, "Cabnet: Category attention block for imbalanced diabetic retinopathy grading," *IEEE Trans. Med. Imaging*, vol. 40, no. 1, pp. 143–153, 2020.

[8] W. X. Lim, Z. Chen, and A. Ahmed, "The adoption of deep learning interpretability techniques on diabetic retinopathy analysis: a review," *Med. Biol. Eng. Comput.*, vol. 60, no. 3, pp. 633–642, 2022.

[9] Selvachandran, S. G. Quek, R. Paramesran, W. Ding, and L. H. Son, "Developments in the detection of diabetic retinopathy: a state-of-the-art review of computer-aided diagnosis and machine learning methods," *Artif. Intell. Rev.*, vol. 56, no. 2, pp. 915–964, 2023.

[10] Khan, S. M. Islam, and R. Ali, "A novel deep learning framework for automatic detection and grading of diabetic retinopathy," *Expert Syst. Appl.*, vol. 206, p. 117827, 2022.

[11] J. M. Shamrat et al., "An advanced deep neural network for fundus image analysis and enhancing diabetic retinopathy detection," *Healthcare Analytics*, vol. 5, p. 100303, 2024.

[12] U. Nneji et al., "Identification of diabetic retinopathy using weighted fusion deep learning based on dual-channel fundus scans," *Diagnostics*, vol. 12, no. 2, p. 540, 2022.

[13] T. Palaniswamy and M. Vellingiri, "Internet of Things and deep learning enabled diabetic retinopathy diagnosis using retinal fundus images," *IEEE Access*, vol. 11, pp. 27590–27601, 2023.

[14] Jabbar et al., "A lesion-based diabetic retinopathy detection through hybrid deep learning model," *IEEE Access*, 2024.

[15] K. Parthiban and M. Kamarasan, "Diabetic retinopathy detection and grading of retinal fundus images using coyote optimization algorithm with deep learning," *Multimed. Tools Appl.*, vol. 82, no. 12, pp. 18947–18966, 2023.

[16] Bilal, L. Zhu, A. Deng, H. Lu, and N. Wu, "AI-based automatic detection and classification of diabetic retinopathy using U-Net and deep learning," *Symmetry*, vol. 14, no. 7, p. 1427, 2022.

[17] M. R. Shoaib et al., "Deep learning innovations in diagnosing diabetic retinopathy: the potential of transfer learning and the DiaCNN model," *Comput. Biol. Med.*, vol. 169, p. 107834, 2024.

[18] P. K. Jena et al., "A novel approach for diabetic retinopathy screening using asymmetric deep learning features," *Big Data Cogn. Comput.*, vol. 7, no. 1, p. 25, 2023.

[19] Shah et al., "Comparative analysis of median filter and its variants for removal of impulse noise from gray scale images," *J. King Saud Univ. Comput. Inf. Sci.*, vol. 34, no. 3, pp. 505–519, 2022.

[20] K. S. Rao et al., "Intelligent ultrasound imaging for enhanced breast cancer diagnosis: ensemble transfer learning strategies," *IEEE Access*, 2024.

[21] Y. Li, J. Zhang, Y. Yan, Y. Lei, and C. Yin, "Enhancing network intrusion detection through the application of the Dung Beetle optimized fusion model," *IEEE Access*, 2024.

[22] M. S. Malik et al., "DeepMedFeature: An accurate feature extraction and drug-drug interaction model for clinical text in medical informatics," *ACM Trans. Asian Low-Resour. Lang. Inf. Process.*, 2024.

[23] Kaggle Dataset: "Diabetic retinopathy 224x224 Gaussian filtered." Available: https://www.kaggle.com/datasets/sovitrath/diabetic-retinopathy-224x224-gaussian-filtered.